22 June 2001

Chemical Physics Letters 341 (2001) 329–337

CHEMICAL PHYSICS LETTERS

www.elsevier.nl/locate/cplett

Multi-dimensional vibrational spectroscopy measured from different phase-matching conditions

Tsuyoshi Kato, Yoshitaka Tanimura *

Institute for Molecular Science Myodaiji, Okazaki, Aichi 444-8585, Japan

Received 12 March 2001; in final form 12 April 2001

Abstract

We developed a theoretical method that can systematically treat the phase-matching condition of nonlinear infrared or Raman measurements. This method might be a rational tool for the analysis of observed signals from various directions based on the response function especially under non-impulsive excitation. Model calculations of the third-order nonlinear IR spectroscopy for a Brownian harmonic oscillator system are performed. We discuss the variation of signals that depend on the observation direction and the temporal width of excitation pulse in comparison with the behavior within the impulsive limit approximation. © 2001 Elsevier Science B.V. All rights reserved.

1. Introduction

The fundamental aim of time-resolved vibrational spectroscopies is to observe various optical responses of the system, which reflect the dynamics of molecular vibrations in condensed phases, collective motions of liquids, solvent reorganization motions, structural change of proteins in biological systems and so on, to construct physical pictures of the underlying dynamical processes.

Since the theoretical proposal of the higher-order ultrafast two-dimensional off-resonant Raman spectroscopy [1,2], considerable experimental and theoretical investigations have been made [3–19] to model the vibrational properties and dynamics in ultrafast time region. Raman measurements are by no means the only method for obtaining vibrational information. An alternative route will be to use infrared pulses to probe the molecular vibrational transition directly [11,12,20]. Recent technological advances to generate femtosecond terahertz pulses by exciting the photocarriers in semiconductor wafer enabled the far-infrared analog of time-resolved Raman spectroscopies to be applicable for the low-frequency vibrational modes in condensed phases [21]. Time-resolved nonlinear IR spectroscopies are direct means to access the molecular vibrations in the electronic ground state and are supposed to provide complement information on the vibrational dynamics to the Raman spectroscopy [2,11,12,22,23].

In practice, to describe the vibrational properties and dynamical responses such as the vibrational anharmonicity and time-scales of relaxation, detailed analysis of the experimental data with the aid of the theoretical response function calculation has to be done. Either Raman or IR spectroscopy, the optical signals may be generated in various phase-matched directions from a sample according

* Corresponding author. Tel.: +81-564-55-7311; Fax: +81-564-53-4660.

E-mail address: tanimura@ims.ac.jp (Y. Tanimura).

0009-2614/01/$ - see front matter © 2001 Elsevier Science B.V. All rights reserved.
PII: S0009-2614(01)00466-3

to the configurations of the incident pulses in nonlinear spectroscopies. Therefore, comparisons from a viewpoint of the variations of the experimental signals emitted into possible directions to the theoretical predictions would provide additional tool for the modeling [24]. In this Letter, we propose a systematic method to calculate optical signals into various phase-matching directions within a perturbative treatment that is applicable to various nonlinear optical spectroscopies. In Section 2, the three-pulse third-order nonlinear IR spectroscopy is described as an example, starting from a basic formula based on the nonlinear response function description. In Section 3, model calculations of third-order nonlinear spectroscopies with two and three incident pulses for a Brownian oscillator system are performed to demonstrate the performance of our method and we examine the variation of signals that depend on the observation direction and the excitation pulse temporal width in comparison with the behavior within the impulsive limit approximation.

2. Theory

2.1. Evaluation of directionally separated signals

In this subsection, we show how the induced nonlinear polarizations can be separated according to their phase-matching directions. Here, as an example, we shall describe the third-order nonlinear spectroscopy which uses three incident infrared laser pulses within a perturbative treatment. The total external electric field is given by

$$E(t) = \sum_{j=1}^{3} E_j(t), \tag{1a}$$

where

$$E_j(t) = \mathscr{E}_j(t)\exp\{\mathrm{i}(k_j \cdot r - \Omega_j t)\} + \text{c.c.} \tag{1b}$$

and $\mathscr{E}_j(t)$, k_j and Ω_j denote, respectively, the pulse envelope function, the wave vector and the angular frequency of jth laser field ($j = 1$, 2 and 3). The wave vectors are assumed not to be collinear with each other. The third-order *total* nonlinear polarization, $P(t)$, is formally calculated by using the third-order nonlinear response function [25] as

$$P(t) = \left(\frac{i}{\hbar}\right)^3 \int_0^\infty \mathrm{d}\tau_3 \int_0^\infty \mathrm{d}\tau_2 \int_0^\infty \mathrm{d}\tau_1 E(t-\tau_3) \times E(t-\tau_3-\tau_2)E(t-\tau_3-\tau_2-\tau_1) \times R^{(3)}(\tau_3,\tau_2,\tau_1) \tag{2a}$$

with

$$R^{(3)}(\tau_3,\tau_2,\tau_1) = \mathrm{Tr}\{[[[\mu(\tau_3+\tau_2+\tau_1), \mu(\tau_2+\tau_1)], \mu(\tau_1)], \mu(0)]\rho_{\mathrm{eq}}\}, \tag{2b}$$

where $\mu(\tau)$ and ρ_{eq} represent, respectively, the dipole operator μ in the interaction picture at time τ and the canonical density operator of the system.

In the corresponding seventh-order off-resonant Raman experiments, the total electric field is expressed as

$$E(t) = \sum_{j=1}^{3} E_j(t) + E_{\mathrm{T}}(t), \tag{3a}$$

where

$$E_j(t) = \mathscr{E}_j(t)\{\exp\{\mathrm{i}(k_j \cdot r - \Omega_j t)\} + \exp\{\mathrm{i}(k'_j \cdot r - \Omega'_j t)\}\} + \text{c.c.} \tag{3b}$$

and $E_{\mathrm{T}}(t)$ is the probe pulse that generates the signal,

$$E_{\mathrm{T}}(t) = \mathscr{E}_{\mathrm{T}}(t)\exp\{\mathrm{i}(k_{\mathrm{T}} \cdot r - \Omega_{\mathrm{T}} t)\} + \text{c.c.} \tag{3c}$$

The seventh-order total nonlinear polarization is expressed as

$$P(t) = \left(\frac{\mathrm{i}}{\hbar}\right)^3 \int_0^\infty \mathrm{d}\tau_3 \int_0^\infty \mathrm{d}\tau_2 \times \int_0^\infty \mathrm{d}\tau_1 E_{\mathrm{T}}(t)E(t-\tau_3)^2 \times E(t-\tau_3-\tau_2)^2 E(t-\tau_3-\tau_2-\tau_1)^2 \times R^{(7)}(\tau_3,\tau_2,\tau_1), \tag{4a}$$

with the response function defined by

$$R^{(7)}(\tau_3,\tau_2,\tau_1) = \mathrm{Tr}\{[[[\alpha(\tau_3+\tau_2+\tau_1), \alpha(\tau_2+\tau_1)], \alpha(\tau_1)], \alpha(0)]\rho_{\mathrm{eq}}\}, \tag{4b}$$

where $\alpha(\tau)$ represents the polarizability operator in the interaction picture. Because the electronically off-resonant optical fields are used, the square of

the field appeared in Eq. (4a) is approximated as [2,25]

$$E(t)^2 \approx 4\sum_j^3 \mathscr{E}_j(t)^2 + 2\sum_j^3 \mathscr{E}_j(t)^2 \times \Big[\exp\{\mathrm{i}[(k_j - k'_j)\cdot r - (\Omega_j - \Omega'_j)t)]\} + \mathrm{c.c.}\Big] + \sum_{i\neq j}^3 \mathscr{E}_i(t)\mathscr{E}_j(t)\Big[\exp\{\mathrm{i}[(k_i - k_j)\cdot r - (\Omega_i - \Omega_j)t)]\} + \exp\{\mathrm{i}[(k'_i - k'_j)\cdot r - (\Omega'_i - \Omega'_j)t)]\} + 2\exp\{\mathrm{i}[(k_i - k'_j)\cdot r - (\Omega_i - \Omega'_j)t)]\} + \mathrm{c.c.}\Big]. \tag{5}$$

The formal appearance of $E(t)^2$ term is similar to that of the $E(t)$ term in Eq. (2a) when we regard $E(t)^2$ term as being composed of a spatially uniform component (the first term on the right-hand side of Eq. (5)) and propagating components (the second and third terms). If pulse pairs are well separated in time, we can neglect the cross terms $\mathscr{E}_i(t)\mathscr{E}_j(t)$ $(i \neq j)$, and differences of wave vectors $\Delta k_j = k_j - k'_j$ and frequencies $\Delta\Omega_j = \Omega_j - \Omega'_j$ appeared in Eq. (5) play the same role as $\{k_j\}$ and $\{\Omega_j\}$ in Eq. (1b), respectively. Thus, in general we can apply the same method as described below for the Nth-order IR spectroscopy to the $(2N+1)$th-order off-resonant Raman spectroscopy. For simplicity, we will investigate third-order IR spectroscopies in this Letter.

By considering the third power of the electric field given by Eq. (1a), one can easily count the number of independent phase-matching directions for the induced polarizations. There are $n = 22$ independent phase-matched directions, κ_j $(j = 1, 2, \ldots, n)$, which are summarized in Table 1. The third-order total nonlinear polarization may be written in the form of

$$P(t) = \sum_{j=1}^n \tilde{P}_j(t)\mathrm{e}^{\mathrm{i}\phi_j} + \mathrm{c.c.}, \tag{6}$$

where $\phi_j \equiv \kappa_j \cdot r$ and $\tilde{P}_j(t)$ denote the spatial phase and the induced polarization component along with the jth direction, respectively. Note that the value of the total nonlinear polarization depends on the choice of wave vectors but those of the polarization components do not. This is the point for the argument below. The expression of Eq. (6) is common one, however, it has been actively utilized by Seidner et al. [26,27] to study directional dependence of optical response for electronic excited state modeled by a two-level system within the rotating-wave approximation (RWA). In order to pull out individual polarization component from the total nonlinear polarization, we rewrite Eq. (6) into a matrix form of

$$\boldsymbol{P}(t) = \boldsymbol{C}\cdot\tilde{\boldsymbol{P}}(t) \tag{7a}$$

with the total polarization vector being

$$\boldsymbol{P}(t) = (P_{s=1}(t), P_2(t), \ldots, P_{2n}(t))^t, \tag{7b}$$

the polarization component vector being

$$\tilde{\boldsymbol{P}}(t) = \Big(\tilde{P}_{j=1}(t), \tilde{P}_2(t), \ldots, \tilde{P}_n(t), \tilde{P}_1^*(t), \tilde{P}_2^*(t), \ldots, \tilde{P}_n^*(t)\Big)^t \tag{7c}$$

and the $(2n \times 2n)$ coefficient matrix $\boldsymbol{C}$ defined as

$$(\boldsymbol{C})_{s,j} = \begin{cases} \exp[+\mathrm{i}\phi_j^{(s)}] & (1 \leqslant j \leqslant n), \\ \exp[-\mathrm{i}\phi_{j-n}^{(s)}] & (n+1 \leqslant j \leqslant 2n). \end{cases} \tag{7d}$$

In Eq. (7d), the integer argument s $(1 \leqslant s \leqslant 2n)$ specifies a certain set of spatial phases $\{\phi_j\}$ generated by a certain choice of the fundamental wave vectors, (k_1, k_2, k_3). For example, if one takes a set of numerical values (v_1, v_2, v_3) for $(k_1\cdot r, k_2\cdot r, k_3\cdot r)$

Table 1
Twenty-two independent phase-matched directions of polarizations induced by interactions with three laser fields with wave vectors k_1, k_2 and k_3

$\kappa_1 = k_1$	$\kappa_2 = k_2$	$\kappa_3 = k_3$	$\kappa_4 = 3k_1$
$\kappa_5 = 3k_2$	$\kappa_6 = 3k_3$	$\kappa_7 = 2k_1 + k_2$	$\kappa_8 = 2k_1 - k_2$
$\kappa_9 = 2k_1 + k_3$	$\kappa_{10} = 2k_1 - k_3$	$\kappa_{11} = 2k_2 + k_1$	$\kappa_{12} = 2k_2 - k_1$
$\kappa_{13} = 2k_2 + k_3$	$\kappa_{14} = 2k_2 - k_3$	$\kappa_{15} = 2k_3 + k_1$	$\kappa_{16} = 2k_3 - k_1$
$\kappa_{17} = 2k_3 + k_2$	$\kappa_{18} = 2k_3 - k_2$	$\kappa_{19} = k_1 + k_2 + k_3$	$\kappa_{20} = k_1 - k_2 + k_3$
$\kappa_{21} = k_1 + k_2 - k_3$	$\kappa_{22} = -k_1 + k_2 + k_3$		

as the sth set, all the spatial phases are generated as $\phi_1^{(s)} = v_1$, $\phi_2^{(s)} = v_2$, $\phi_3^{(s)} = v_3$, $\phi_4^{(s)} = 3v_1$, …, according to the relation in Table 1. The total nonlinear polarization calculated from Eqs. (1a) to (2b) implicitly depends on the choice of the set to give the elements in the total polarization vector of Eq. (7b). If the spatial phases $\{\phi_j^{(s)}\}$ are generated so that the inverse of the coefficient matrix $\boldsymbol{C}$ exists, then the polarization components can be extracted from the total nonlinear polarization by the inversion of Eq. (7a) as,

$$\tilde{\boldsymbol{P}}(t) = \boldsymbol{C}^{-1} \cdot \boldsymbol{P}(t), \tag{8}$$

which is the key expression in this Letter. This relation holds without the RWA and by using this we can properly take into account relative contributions of each quantum pathway to all possible phase-matched signals simultaneously without classifying the quantum pathways by time-orderings of the field-matter interactions and by the type of the vibrational transitions. The selection of quantum pathways is performed though the convolution of the response function with the electric field of the laser pulses depending on the frequencies of lasers and the coordinate dependence of dipole (polarizability) operator. As shown in Section 3, the selection is effective in modifying the signals not only for non-impulsive excitation but also for spectroscopies in which laser pulses recognized as impulsive are utilized.

Essentially the same mathematical procedure is needed for the applications to other nonlinear IR spectroscopies. For example, in the case of spectroscopies that utilize two external fields, k_1 and k_2, including the two-pulse IR echo and the IR pump-probe spectroscopy and so on, we have $n = 8$ independent phase-matched directions (see Table 2).

2.2. Model system

To demonstrate our method, we consider a Brownian harmonic oscillator system [2,11,12,28]. The third-order response function is analytically expressed by using the two-point correlation function of the system coordinate, $C(\tau)$, as

$$\begin{aligned} R^{(3)}(\tau_3,\tau_2,\tau_1) = \frac{32\mathrm{i}\mu_1^2\mu_2^2}{\hbar^3} C(\tau_3)[&C(\tau_2+\tau_1)C(\tau_3+\tau_2) \\ &+ C(\tau_3+\tau_2+\tau_1)C(\tau_2) + C(\tau_3+\tau_2) \\ &C(\tau_1) + C(\tau_2)C(\tau_1)] \end{aligned} \tag{9a}$$

with

$$\begin{aligned} C(\tau) &= \theta(\tau)\frac{\hbar}{2m\zeta}\sin(\zeta\tau)\mathrm{e}^{-\gamma\tau/2}, \\ \zeta &= \sqrt{\omega_0^2 - \gamma^2/4}, \end{aligned} \tag{9b}$$

where ω_0, m and γ are the fundamental frequency, the reduced mass and damping constant $\zeta = \sqrt{\omega_0^2 - \gamma^2/4}$, respectively. We assumed the form of the transition dipole moment as $\hat{\mu} = \mu_1\hat{q} + \mu_2\hat{q}^2$ ($\mu_1 \gg \mu_2$).

3. Numerical results and discussions

In the following calculations, we use $\omega_0/2\pi = 50\ \mathrm{cm}^{-1}$ and $\gamma = 0.1\omega_0$. The carrier frequency of the pulse is taken as $\Omega_j = \omega_0$ ($j = 1$, 2 and 3). We set the pulse sequence as $\mathscr{E}_1(t) = \epsilon_1(t), \mathscr{E}_2(t) = \epsilon_2(t-\tau)$ and $\mathscr{E}_3(t) = \epsilon_3(t - |\tau| - T)$ with the Gaussian envelope function, $\epsilon_j(t)$, being $\epsilon_j(t) = A_j/(\sqrt{2\pi}\sigma_j)\exp[-t^2/(2\sigma_j^2)]$, where A_j denotes the amplitude. We assume weak probe pulses and set $A_2/A_1 = A_3/A_1 = 0.5$, and the same pulse width (fwhm) $\Delta_{\mathrm{pulse}} \equiv \sqrt{8\log 2}\sigma_j$ for all j. Among infinite sets of spatial phases that make the coefficient matrix $\boldsymbol{C}$ nonsingular, we use a parameter set, $\phi_1^{(s)} = \eta_1 s$, $\phi_2^{(s)} = \eta_2 s$, $\phi_3^{(s)} = \eta_3 s, \ldots$ with constants $\eta_1 = 2\pi/1.2\times 10^2$, $\eta_2 = 2\pi/1.3$ and $\eta_3 = 2\pi/1.4\times 10^{-2}$. By using this set we obtain matrix elements that are not too large or too small compared with other matrix elements in both $\boldsymbol{C}$ and $\boldsymbol{C}^{-1}$. Other choice of constants η_i ($i = 1, 2, 3$) leads to different elements in $\boldsymbol{P}(t)$ and $\boldsymbol{C}$, however, we

Table 2
Eight independent phase-matched directions of polarizations induced by interactions with two laser fields with wave vectors k_1 and k_2

$\kappa_1 = k_1$	$\kappa_2 = k_2$	$\kappa_3 = 2k_1 - k_2$	$\kappa_4 = 2k_2 - k_1$
$\kappa_5 = 2k_1 + k_2$	$\kappa_6 = 2k_2 + k_1$	$\kappa_7 = 3k_1$	$\kappa_8 = 3k_2$

obtain the same polarization component vector $\tilde{\boldsymbol{P}}(t)$ within the numerical error.

Firstly, we consider the case that utilizes two external fields, k_1 and k_2, in which $n = 8$ independent phase-matched directions summarized in Table 2 are considered. The intensity of the emitted light along with the jth direction at observation time, t_s, is evaluated by calculating the absolute square of the corresponding polarization component, $I_j(t_s;\tau) = |\tilde{P}_j(t_s + |\tau|)|^2$, as a function of the separation τ between the peaks of pulse k_2 and k_1 (which can be negative or positive; $\tau > 0$ means k_1 pulse proceeds k_2 pulse and vice versa). The observation time is measured from the second pulse peak and we set time zero at the peak position of the pulse that arrives at the sample for the first time. The time-integrated signal is defined as $S_j(\tau) = \int_{-\infty}^{\infty} \mathrm{d}t_s I_j(t_s;\tau)$.

In Fig. 1, $S_j(\tau)$ for six phase-matched directions are plotted for pulses with the duration $\Delta_{\text{pulse}} = 300$ fs. These pulses are usually recognized as impulsive since $\Delta_{\text{pulse}} < 2\pi/\omega_0 = 667$ fs and $\Delta_{\text{pulse}} < 1/\gamma = 1.1$ ps. As shown, our method clearly separates the directional signals. The mirror image relations between the signals of $\kappa_3 = 2k_1 - k_2$ and $\kappa_4 = 2k_2 - k_1$, and those of $\kappa_5 = 2k_1 + k_2$ and $\kappa_6 = 2k_2 + k_1$ hold. The signals for the directions $\kappa_7 = 3k_1$ and $\kappa_8 = 3k_2$ are omitted because they show no τ dependence as should be; signals are generated by interactions with either k_1 or k_2 pulse alone. It is found that in the two-pulse photon echo direction, $\kappa_4 = 2k_2 - k_1$, the signal changes its oscillation frequency at about ω_0 for negative τ to $2\omega_0$ for positive τ. This frequency change is not predicted by the impulsive limit approximation, $\mathscr{E}(t) \propto \delta(t)$, which results in the oscillation at $2\omega_0$ for both negative and positive τ. This is a possible breakdown of the impulsive limit approximation even for the use of short pulses that are usually regarded as impulsive. One obtains $\tilde{P}_{\kappa_4}(t_s + |\tau|) \propto R^{(3)}(t_s, |\tau|, 0)$ for negative τ within the impulsive approximation where zero in the response function comes from the assumption that the pulse duration is infinitesimal. Actually we observe the frequency modulation in the signal from ω_0 to $2\omega_0$ by using $R^{(3)}(t_s, |\tau|, \epsilon)$ with $\epsilon = 100$ fs instead.

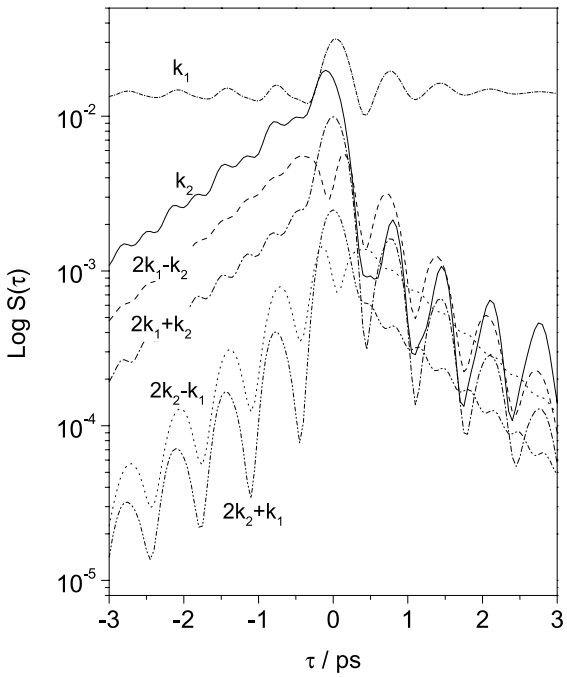

Fig. 1. Time-integrated signals for six phase-matched directions in the two-pulse nonlinear spectroscopy for pulses with $\Delta_{\text{pulse}} = 300$ fs. The corresponding phase-matched wave vectors are depicted (see text and Table 2 for details).

By converting from time-domain to frequency-domain, discrepancy of the impulsive approximation from the present results becomes apparent. We consider the frequency-domain photon echo technique and the dispersed pump–probe spectroscopy. The frequency-domain photon echo signal corresponds to observe the absolute square of the Fourier transform of the emitted field along with the photon echo phase-matched direction. Such experiment has been done by use of the IR stimulated photon echo configuration to investigate the anharmonicity and level-dependent dephasing time in molecular vibrations [23,29]. Here, we calculate signals for the two-pulse photon echo analog of such experiments. By using the Fourier transform of the polarization component, $\tilde{P}_{2k_2-k_1}[\omega] = \int_{-\infty}^{\infty} \mathrm{d}t\, \mathrm{e}^{\mathrm{i}\omega t} \tilde{P}_{2k_2-k_1}(t)$, we obtain the frequency-domain photon echo signal as $I_{2k_2-k_1}(\omega;\tau) = |\tilde{P}_{2k_2-k_1}[\omega]|^2$. The dispersed pump–probe spectrum is calculated by the formula [25,30], $S(\omega;\tau) = \omega\, \mathrm{Im}(E_2(\omega)\tilde{P}^*_{k_2}[\omega])$, where $E_2(\omega)$ is the Fourier transform of the probe pulse $E_2(\omega) =$

$\int_{-\infty}^{\infty} \mathrm{d}t\ \exp\{\mathrm{i}(\omega - \Omega_2)t\}\mathscr{E}_2(t)$, and the sign convention is such that the signal is negative for absorption. (As has already been pointed out by Park and Cho [31], direct applications of these formulae may fail in describing *real* observables for the THz pulse experiments since the slowly varying approximation cannot be adopted, however, they are useful for the sake of demonstration purpose.)

In Fig. 2a,b we plot $I_{2k_2-k_1}(\omega;\tau)$ and $S(\omega;\tau)$, respectively, in comparison with signals calculated by using the impulsive limit approximation. Both results show the signals at about $\omega/2\pi = 50\ \mathrm{cm}^{-1}$ if we do not apply the impulsive approximation. Apparently, they are brought about by the finiteness of the pulse duration, and they remain even for the shorter pulse duration $\Delta_{\mathrm{pulse}} = 100$ fs. It can be shown that both spectroscopies have resonances at $\omega = 0, \pm 2\zeta$ in the impulsive limit. We observe signals at $\zeta/2\pi \approx 50\ \mathrm{cm}^{-1}$ by substituting $\epsilon = 100$ fs for zero in the relevant response functions as mentioned for the time-integrated signal. The suppression of the signal at $\omega/2\pi = 0\ \mathrm{cm}^{-1}$ for $S(\omega;\tau)$ (Fig. 2b) is due to the factor ω in the definition above. In the long pulse duration case, $\Delta_{\mathrm{pulse}} = 900$ fs, the main portion of the signal is at $\omega/2\pi \approx 50\ \mathrm{cm}^{-1}$, which is required by the conservation of energy.

Next, we consider the three-pulse spectroscopy, where the third pulse k_3 is applied in addition to the previous two. Accordingly we have another time period $T(\geqslant 0)$, the separation of the second pulse peak and the k_3 pulse peak, which can be handled experimentally. The intensity of the emitted light along with the jth direction at the observation time, t_s, is defined by $I_j(t_s;\tau,T) =$

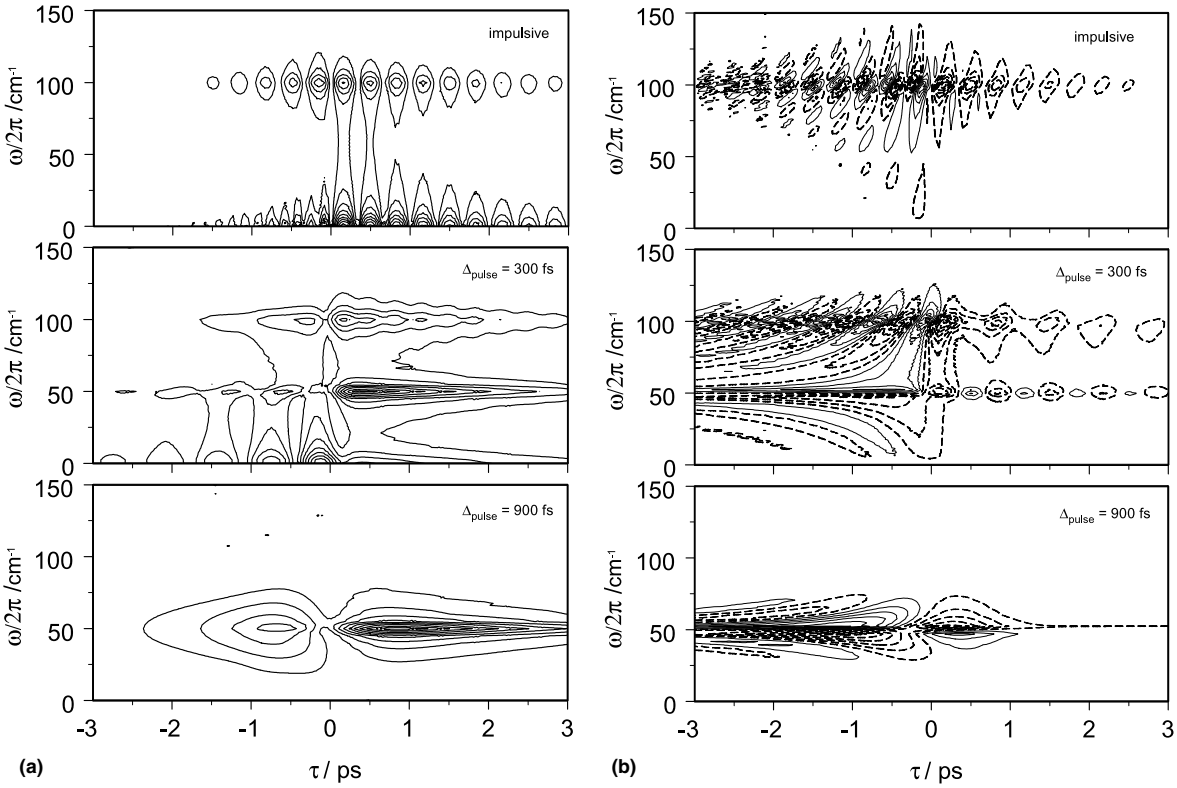

Fig. 2. Contour plot of calculated (a) frequency-domain two-pulse photon echo signals and (b) dispersed pump–probe signals. In both figures the upper panel shows the signal calculated by the impulsive limit approximation, while the middle and the lower one show for the pulse duration $\Delta_{\mathrm{pulse}} = 300$ and 900 fs, respectively. In Fig. 2b, dashed lines show the negative signal.

$|\tilde{P}_j(t_s + |\tau| + T)|^2$, as a function of the separation τ and T where the observation time is measured from the k_3 pulse peak. The time-integrated signal is also defined as $S_j(\tau, T) = \int_{-\infty}^{\infty} \mathrm{d}t_s I_j(t_s; \tau, T)$.

We calculated $S_j(\tau, T)$ for the phase-matched directions into which the scattering light proportional to $A_1A_2A_3$ are emitted, e.g., four directions from κ_{19} to κ_{22} in Table 1. In the left column of Fig. 3, the results for the pure homogeneous system are plotted. The signals of $\kappa_{19} = k_1 + k_2 + k_3$ and $\kappa_{21} = k_1 + k_2 - k_3$ directions are symmetric with respect to $\tau = 0$ ps axis, while those of $\kappa_{20} = k_1 - k_2 + k_3$ (not shown) and $\kappa_{22} = -k_1 + k_2 + k_3$ directions are asymmetric. This comes from the sign of k_1 and k_2 wave vectors; in the former the signs of two wave vector are the same, while in the latter they have opposite sign. This means that even in the interaction with relatively short pulses the two components of the field-matter dipole interaction term, $\hat{\mu}\mathscr{E}(t)\exp\{-\mathrm{i}(k \cdot r - \omega t)\}$ and $\hat{\mu}\mathscr{E}(t)\exp\{+\mathrm{i}(k \cdot r - \omega t)\}$, have relative importance and the impulsive limit approximation breaks down in which two components possess the same role. The static inhomogeneous effect of the vibrational frequency is easily taken into account by averaging the response function of Eq. (9a) with the Gaussian

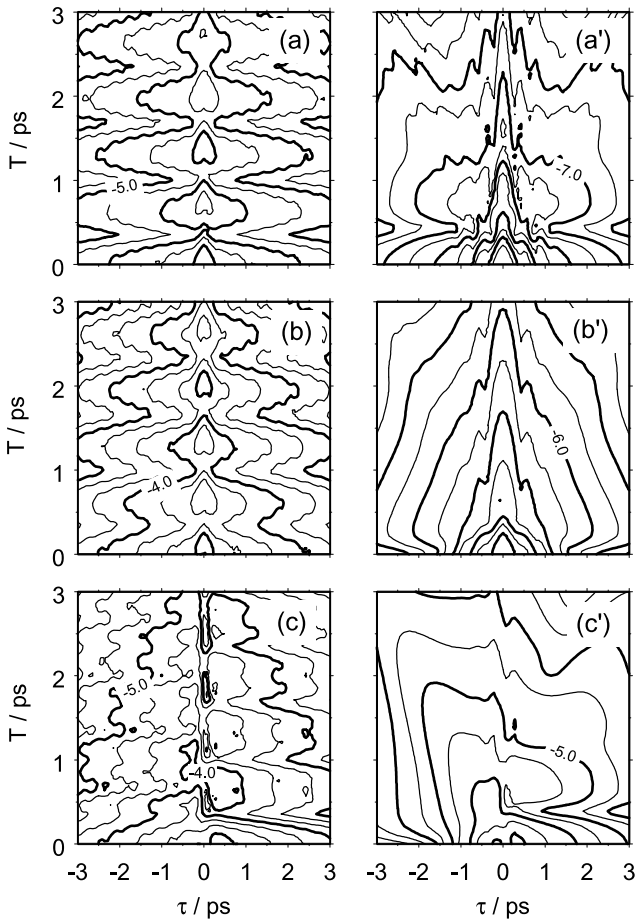

Fig. 3. Contour plots of logarithm of $S(\tau, T)$ for three phase-matched directions; (a) $\kappa_{19} = k_1 + k_2 + k_3$, (b) $\kappa_{21} = k_1 + k_2 - k_3$ and (c) $\kappa_{22} = -k_1 + k_2 + k_3$. The left column shows the homogeneous case, while the right column shows the signals from the system with static inhomogeneity. (The signal for $\kappa_{20} = k_1 - k_2 + k_3$ is the mirror image of (c) with respect to the $\tau = 0$ ps axis.) The pulse duration is $\Delta_{\mathrm{pulse}} = 300$ fs. Each signal has the maximum value at around the origin and the spacing between adjacent thick lines is 1.

distribution function of the fundamental frequency, $S(\omega_0) \propto \theta(\omega_0)\exp[-(\omega_0 - \bar{\omega}_0)^2/(2\sigma_\omega^2)]$, where $\bar{\omega}_0$ denotes the center of the distribution, and the width (fwhm) of the broadening is given by $\Delta_\omega \equiv \sqrt{8\log 2}\sigma_\omega$. In the right column of Fig. 3, we show the same signals from the system with static inhomogeneity $\Delta_\omega/2\pi = 20\ \mathrm{cm}^{-1}$ for $\bar{\omega}_0/2\pi = 50\ \mathrm{cm}^{-1}$. Again, the signals along with the κ_{19} and κ_{21} directions are symmetric with $\tau = 0$ ps axis, but their apparent similarity in the pure homogeneous case is lost. Signals in κ_{19} and the stimulated photon echo direction, κ_{22}, show correlation along with $T = |\tau|$ line as the photon echo signal from an inhomogeneously broadened two-level system. It is not apparent that the system shows such correlations because the system is not just a two-level system. Detailed analysis of such an echo behavior needs further study.

We find it necessary to mention about the reduction of the calculations depending on the required phase-matched directions. In the three incident pulse case, if one only needs the polarization components proportional to $A_1A_2A_3$ as demonstrated above, namely four directions from κ_{19} to κ_{22}, the dimensions of the matrices $\boldsymbol{C}$ and $\boldsymbol{C}^{-1}$ are reduced to $4 \times 2 = 8$ since other polarization components do not couple with these components, although it is needed to exclude the contribution that are not proportional to $A_1A_2A_3$ in evaluating the integration of Eq. (2a). Similarly, in the two-pulse case the dimension of matrices are reduced to 12 for the calculation of the signals that are proportional to $A_1^2A_2$ and $A_1A_2^2$.

Finally, we mention about experiments where electronically off-resonant Raman transition(s) is involved as well as IR transitions. In this case we need to evaluate several response functions according to the chronological order of the field-matter interactions [32–35] and to perform time-integrations as Eqs. (2a) and (4a) for each response function. It is straightforward to apply our method to such experiments to separate the signals by the phase-matching directions, however, the procedure will be complicated.

In conclusion we proposed a systematic scheme to calculate the directionally separated signals for nonlinear vibrational spectroscopies. Calculations of the two- and three-pulse nonlinear spectroscopy for a Brownian harmonic oscillator model were performed and we demonstrated the variation of signals depending on the observation direction and the excitation pulse temporal width to show possible break downs of impulsive limit approximation. We emphasize that the comparisons of experimental signals observed from various phase-matched directions and theoretical predictions would make it more feasible to model the vibrational dynamics in condensed phases once the nonlinear response function is obtained, although there is another need to treat the tensoral properties of the response function. We are planning to calculate directionally resolved signals by using the method proposed in this Letter from vibrational systems coupled to the bath degree of freedom by nonlinear coordinate interactions, in which higher-order response functions are reported to show echo-like behaviors [36].

References

[1] R.F. Loring, S. Mukamel, J. Chem. Phys. 83 (1985) 2116.
[2] Y. Tanimura, S. Mukamel, J. Chem. Phys. 99 (1993) 9496.
[3] D.V. Bout, L.J. Muller, M. Berg, Phys. Rev. Lett. 67 (1991) 3700.
[4] R. Inaba, K. Tominaga, M. Tasumi, K.A. Nelson, K. Yoshihara, Chem. Phys. Lett. 211 (1993) 183.
[5] K. Tominaga, K. Yoshihara, Phys. Rev. Lett. 74 (1995) 3061.
[6] T. Steffen, K. Duppen, Phys. Rev. Lett. 76 (1996) 1224.
[7] D.A. Blank, L.J. Kaufman, G.R. Fleming, J. Chem. Phys. 111 (1999) 3105.
[8] V. Astinov, K.J. Kubarych, C.J. Milne, R.J.D. Miller, Chem. Phys. Lett. 327 (2000) 334.
[9] O. Golonzka, N. Demirdöven, M. Khalil, A. Tokmakoff, J. Chem. Phys. 113 (2000) 9893.
[10] D.A. Blank, L.J. Kaufman, G.R. Fleming, J. Chem. Phys. 113 (2000) 771.
[11] V. Khidekel, S. Mukamel, Chem. Phys. Lett. 204 (1995) 304.
[12] V. Khidekel, S. Mukamel, Chem. Phys. Lett. 263 (1996) 350.
[13] T. Steffen, J.T. Fourkas, K. Duppen, J. Chem. Phys. 105 (1996) 7364.
[14] K. Okumura, Y. Tanimura, J. Chem. Phys. 107 (1997) 2267.
[15] T. Steffen, K. Duppen, Chem. Phys. 223 (1998) 267.
[16] J. Sung, M. Cho, J. Chem. Phys. 113 (2000) 7072.
[17] S. Saito, I. Ohmine, J. Chem. Phys. 108 (1998) 240.
[18] R.L. Murry, J.T. Fourkas, T. Keyes, J. Chem. Phys. 109 (1998) 7913.

[19] A. Ma, R.M. Stratt, Phys. Rev. Lett. 85 (2000) 1004.
[20] D. Zimdars, A. Tokmakoff, S. Chen, S.R. Greenfield, M.D. Fayer, Phys. Rev. Lett. 70 (1993) 2718.
[21] G. Haran, W.D. Sun, K. Wynne, R.M. Hochstrasser, Chem. Phys. Lett. 274 (1997) 365.
[22] P. Hamm, M. Lim, R.M. Hochstrasser, Phys. Rev. Lett. 81 (1998) 5326.
[23] M.C. Asplund, Mt.T. Zanni, R.M. Hochstrasser, Proc. Nat. Acad. Sci. 97 (2000) 8219.
[24] W.M. Zhang, V. Chernyak, S. Mukamel, J. Chem. Phys. 110 (1999) 5011.
[25] For example S. Mukamel, Principles of Nonlinear Optical Spectroscopy, Oxford University Press, Oxford, 1995.
[26] L. Seidner, G. Stock, W. Domcke, J. Chem. Phys. 103 (1995) 3998.
[27] B. Wolfseder, L. Seidner, G. Stock, W. Domcke, Chem. Phys. Lett. 217 (1997) 275.
[28] K. Okumura, Y. Tanimura, J. Chem. Phys. 106 (1997) 1687.
[29] M.C. Asplund, M. Lim, R.M. Hochstrasser, Chem. Phys. Lett. 323 (2000) 269.
[30] G. Stock, W. Domcke, Phys. Rev. A 45 (1992) 3032.
[31] K. Park, M. Cho, J. Chem. Phys. 109 (1998) 10559.
[32] W. Zhao, J. Wright, J. Am. Chem. Soc. 121 (1999) 10994.
[33] W. Zhao, J. Wright, Phys. Rev. Lett. 83 (1999) 1950.
[34] M. Cho, Two-dimensional vibrational spectroscopy, in: S.H. Lin, A.A. Villaeys, Y. Fujimura (Eds.), Advances in Multiphoton Process and Spectroscopy, World Scientific, Singapore, vol. 12, 1999, p. 229.
[35] K. Park, M. Cho, J. Chem. Phys. 112 (2000) 5021.
[36] Y. Tanimura, T. Steffen, J. Phys. Soc. Jpn. 69 (2000) 4095.